Robust Estimation of 5-ALA Induced PpIX Multiple-Wavelength Excitation Fluorescence Spectroscopy for Improving Glioma Classification

Arthur Gautheron, Michaël Sdika, Mathieu Hébert, Bruno Montcel

▶ **To cite this version:**

Arthur Gautheron, Michaël Sdika, Mathieu Hébert, Bruno Montcel. Robust Estimation of 5-ALA Induced PpIX Multiple-Wavelength Excitation Fluorescence Spectroscopy for Improving Glioma Classification. SPIE Photonics Europe, Clinical Biophotonics II ; SPIE proceedings, Apr 2022, Strasbourg, France. pp.1214607, 10.1117/12.2620945 . hal-03665499

HAL Id: hal-03665499
https://hal.science/hal-03665499v1

Submitted on 11 May 2022

HAL is a multi-disciplinary open access archive for the deposit and dissemination of scientific research documents, whether they are published or not. The documents may come from teaching and research institutions in France or abroad, or from public or private research centers.

L'archive ouverte pluridisciplinaire **HAL**, est destinée au dépôt et à la diffusion de documents scientifiques de niveau recherche, publiés ou non, émanant des établissements d'enseignement et de recherche français ou étrangers, des laboratoires publics ou privés.

Robust Estimation of 5-ALA Induced PpIX Multiple-Wavelength Excitation Fluorescence Spectroscopy for Improving Glioma Classification

A. Gautheron[a], M. Sdika[a], M. Hébert[b], and B. Montcel[a]

[a]Univ Lyon, INSA-Lyon, Université Claude Bernard Lyon 1, CNRS, Inserm, CREATIS UMR 5220, U1206, F-69621, LYON, France
[b]Univ Lyon, UJM-Saint-Etienne, CNRS, Institut d Optique Graduate School, Lab. Hubert Curien UMR 5516, F-42023, St Etienne, France

ABSTRACT

Protoporphyrin IX (PpIX) is a fluorophore now used to identify tumoral tissues. The tissue is usually excited at one wavelength, e.g., 405 nm, and the fluorescence signal generated by this molecule and other fluorophores (the baseline) is used to estimate the amount of PpIX. However, fluorophores too close to PpIX impair the estimation and resulting classifications. Thus, we handle this issue by suggesting an efficient multi-excitation wavelengths method, free from any *a priori* on the baseline. Our method aims to distinguish healthy tissues from tumor margins, while being more robust to baseline variability. It keeps an ability to distinguish healthy from tumor tissues up to 87% in cases where existing methods'ability drops near 0%.

Keywords: 5-ALA, fluorescence spectroscopy, glioma, Protoporphyrin IX, classification, neurosurgery

1. INTRODUCTION

Still hardly curable today, diffuse gliomas account for more than fifty percent of primitive brain tumors. Most studies commonly consider two separate groups having different biological, molecular and tissue properties: High Grade Gliomas (HGG) are mainly malignant tumors and Low Grade Gliomas (LGG) are begnin tumors. All subtypes of gliomas share the same highly infiltrative behavior of individual tumor cells. However surrounding infiltrated tissue often resemble normal tissues. Pre-operative MRI combined with neuro-navigation is currently used to localize surgical tools and tumour cells in the operating theater but it shows strong limitations.

As a complementary method to pre-operative MRI, fluorescence microscopy has shown its relevance in neuro-oncology[1–5] and 5-aminolevulonic acid (5-ALA) induced fluorescence of protoporphyrin IX (PpIX) is currently used through surgical microscopes.[6] This technique is the current clinical standard for PpIX-based surgical assistance. However, its sensitivity is still limited when applied to low density infiltrative parts of HGG or to LGG. Thus, many 5-ALA induced PpIX spectroscopy methods arise to tackle this issue.[7] The accuracy of this fluorescence spectroscopy methods remains limited by the presence of other non 5-ALA induced fluorophores such as NADH, FAD, flavins or lipopigments. These fluorophores and their high variability can lead to important crosstalks with PpIX.[8–10] To avoid crosstalk, the overall approach is to model the baseline with everything that is not due to 5-ALA-induced PpIX. Existing approaches are effective when the emission spectral band of the baseline is far from the one of the PpIX.[8,11–13] The baseline is modeled by a Gaussian function,[14,15] or expert dependent weighted sum, which contain a finite number of fluorophores whose fluorescence spectral shape is assumed known.[8,16] However, fluorophores that overlap with PpIX spectral emission band are difficult to consider. These important crosstalks largely impact specificity.

In this work, we introduce a novel approach to estimate the PpIX fluorescence-related biomarkers contribution. As opposed to state of the art, several excitation wavelengths are used. This additional input enables to be free

Further author information:
A. Gautheron : E-mail: gautheron@creatis.insa-lyon.fr,
B. Montcel: E-mail: montcel@creatis.insa-lyon.fr

from any *a priori* on the baseline shape. We apply our method in the case of the two forms of PpIX ($PpIX_{620}$, $PpIX_{634}$) using a numerical phantom calibrated on real data.[14,15,17] Our method improves the robustness of the estimation of PpIX contributions. We compare the performance of our method against state of the art by studying confusion matrices of the classification task between healthy tissues and tumor margins.

2. MATERIALS AND METHOD

The fluorescence emission spectrum used in this study relies on multiple excitation wavelengths. At each excitation wavelength λ_e, the fluorescence spectrum S_{λ_e} can be written :

$$m_{\lambda_e} = \alpha_1\eta_1(\lambda_e)S_1 + \alpha_2\eta_2(\lambda_e)S_2 + \gamma(\lambda_e)b \ , \tag{1}$$

where all quantities indexed by 1, *resp. 2*, refer to $PpIX_{620}$, *resp.* $PpIX_{634}$, with S_i the normalized emission spectrum, η_i the quantum yield at excitation wavelength, α_i the contribution of the given PpIX form, and b, named baseline, represents other endogenous fluorophore emission spectra. If we consider two wavelengths λ_e, λ'_e, we can then write:

$$m = \alpha_1\eta_1 S_1 + \alpha_2\eta_2 S_2 + b \quad \text{and} \quad m' = \alpha_1\eta'_1 S_1 + \alpha_2\eta'_2 S_2 + \gamma b \tag{2}$$

where m, m', S_1, S_1, η_1, η_2, η'_1 and η'_2 are given.

We define the interest parameter vector $\alpha = (\alpha_1, \alpha_2)^T$ and the measurement vector $\tilde{m} = (m, m')^T$. To estimate values of α, we define different models. Baseline Free Model (BF) considers that $b = 0$ and $\gamma b = 0$. Gaussian Baseline Model (GB) suggests that $b = A\mathcal{G}(\mu, \sigma)$ and $\gamma b = A'\mathcal{G}(\mu, \sigma)$ where $\mathcal{G}$ is a Gaussian lineshape with mean μ and standard deviation σ. Estimated Baseline Model (EB) has no a priori on b and γb, but it requires to additionally fit γ and b parameters.

In our experiments, we use a digital phantom parameterized from in vivo data.[14,15] We consider two excitation wavelengths λ_e =385 nm and λ'_e =405 nm; the quantum yield ratio for $PpIX_{620}$ is $\rho_1 = \eta'_1/\eta_1 = 1.62$; and for $PpIX_{634}$ it is $\rho_2 = \eta'_2/\eta_2 = 0.76$.[17] To have a more realistic digital phantom, we decided to model acquisition noise. Therefore, we model a noise with two components: a Poisson noise $\mathcal{P}$ mimics photon noise and an additive Gaussian white noise $\mathcal{N}$ mimics electronic noise. This leads to the following function representing the generated spectrum :

$$m = \mathcal{P}\left[\alpha_1\eta_1 S_1 + \alpha_2\eta_2 S_2 + b(\lambda_e)\right] + \mathcal{N} \ , \text{ where } \ b(\lambda_e) = \gamma(\lambda_e)A\frac{2}{\pi\sigma_{para}}\frac{1}{1+\left(\frac{\lambda-\lambda_{para}}{\frac{\sigma_{para}}{2}}\right)^2}. \tag{3}$$

All results given in this work have been computed over 10^5 draws of α couples, equally tesselled into 100x100 bins to map a part of the (α_1,α_2) diagram also called α plane. Each region of the plane is associated with a pathological status, refer to *Alston* et al.[14,15] We focus on the boundary between healthy and tumor tissues, which corresponds to an area of this plane. We used seven baseline datasets which correspond to different scenarios for the application of our method in clinical practice. The simulation parameters are given in Table 1

Name	Parameters
General	$A = \Gamma(4.102, 82.6840)$ u.a. $\mu_{para} = \mathcal{U}(590, 650)$ nm $\sigma_{para} = \mathcal{U}(0, 25)$ nm $\gamma = \mathcal{U}(0.1, 1.125)$
Amplitude (A)	$A = \Gamma(4.102, 826.684)$ u.a.
Width (σ_{para})	$\sigma_{para} = \mathcal{U}(0, 50)$ nm

Name	Parameters
Outside	$\mu_{para} = \mathcal{U}(550, 590)$ nm $\gamma = \mathcal{U}(0.1, 3.00)$
Inside	$\mu_{para} = \mathcal{U}(620, 640)$ nm $\gamma = \mathcal{U}(0.1, 3.00)$
Inner	$\gamma = \mathcal{U}(1, 1.2)$
Across	$\gamma = \mathcal{U}(0.6, 0.8)$

Table 1: Parameters used for the simulation of the seven baseline datasets. Only changes from "General" are given for the six other datasets.

where $\mathcal{U}(a, b)$ is a uniform distribution between a and b, and $\Gamma(k, \beta)$ is a gamma distribution with shape factor k and scale factor β.

To determine the pathological status of each sample according to the estimated parameters α^*, we use a bayesian classifier. It splits LGG from HGG and uses *a priori* knowledge on categories given by *Alston* et al.[15] We apply this classifier on simulated glioma images which contains a tumor and a healthy region. To have a more realistic experiment, we account for the spatial point spread function of the probe: results are convolved with a Gaussian kernel of size 30x30 pixels.

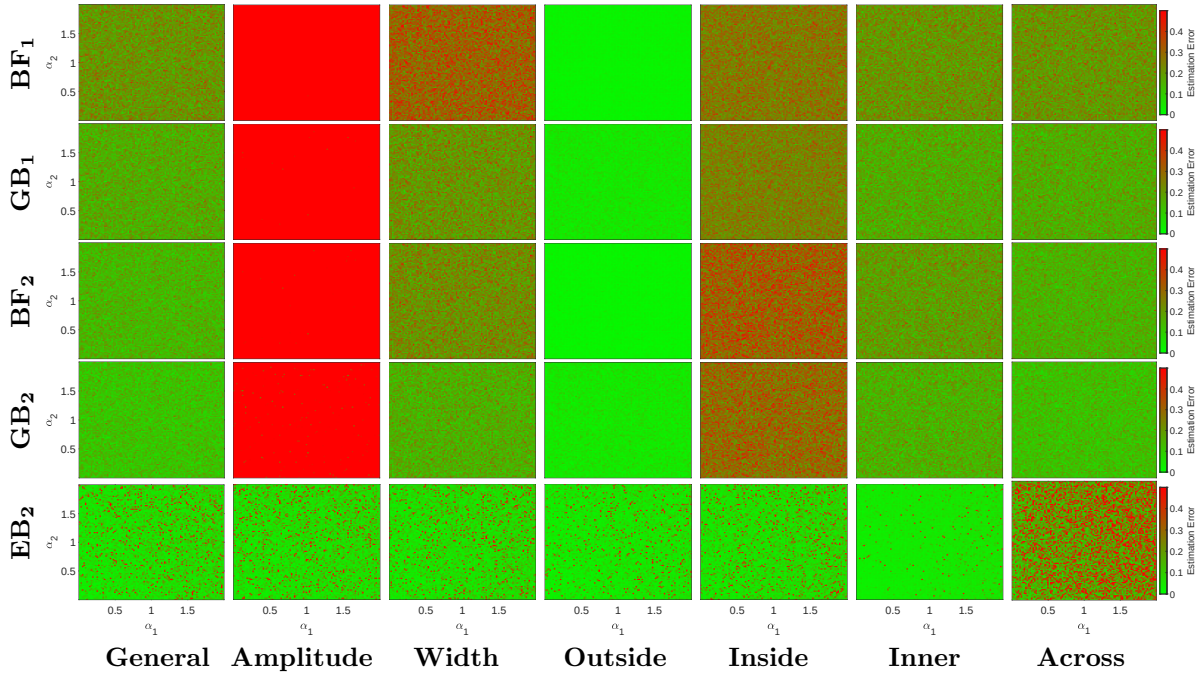

Figure 1: Map of (α_1, α_2) absolute estimation Error for each estimation method in row : Baseline Free (BF), Gaussian Baseline (GB), and Estimated Baseline (EB). Each column represent the same baseline dataset defined in Table 1. Each map has been computed by 100000 drawings equally split in 100x100 bins. The more red is the color, the greater the absolute error of estimation and the greener the color, the lower the absolute error of estimation.

3. RESULTS AND DISCUSSION

In Fig. 1, one can see the map of α estimation error by each model for all the baseline parameters sets. At first sight, one can notice that EB_2 has a small error for each baseline set except Across. Considering Amplitude, Width and Inside datasets, one can see that EB_2 has the lowest error compared to other models. It highlights the robustness to the baseline's variability of EB_2 compared to state of the art models (BF_1, GB_1) even extrapolated at two excitation wavelengths (BF_2, GB_2). Looking at the Outside dataset, one notice that EB_2 has a greater error than other models, however this dataset refers to a clinical case which is no more an issue. Comparing Inner with Across datasets, we notice that the error of state of the art models remains constant while the one of EB_2 increases a lot. This is due to the EB_2 instability when γ is close to ρ_1 or ρ_2. Because the final aim is to determine the boundary between healthy tissues and margins, we simplify the classification task into two categories: tumoral and healthy.

In Fig. 2, one can see confusion matrices in LGG and HGG for General and Amplitude datasets accounting for the measurement probe. In each confusion matrix, the bottom right corner corresponds to the correctly predicted tumoral category and the top left corner to the correctly predicted healthy category. One can notice that the classification task is an ill-posed problem because anti-diagonal terms of the confusion matrix associated

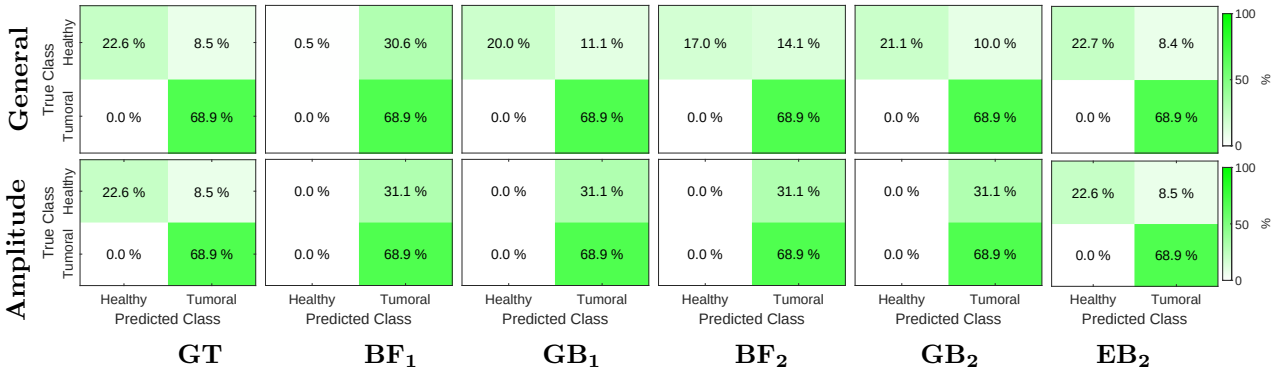

(a) LGG Case

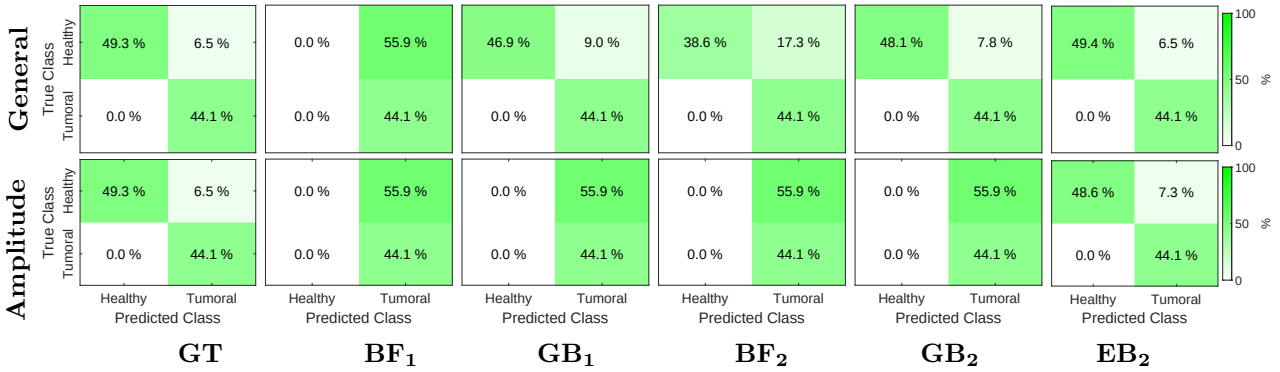

(b) HGG Case

Figure 2: Confusion matrices of healthy/tumoral classification on images of simulated glioma accounting for the spatial point spread function of the probe. In the case of LGG and HGG, each row corresponds to a specific baseline dataset referring to Table 1 and each column to an estimation model. Inside each confusion matrix, each row corresponds to the true class while each column to the predicted class.

to Ground Truth are not zero. In LGG and HGG, for both baseline parameters sets, all models are as performant as the GT for predicting truly tumoral samples. In the General dataset, BF_1 is unable to correctly predict truly healthy samples, and EB_2 has the closest percentage value to GT. Considering Amplitude dataset in both LGG and HGG, only EB_2 is able to correctly predict truly healthy samples. In HGG, only 1.62% of healthy samples are predicted as tumoral with EB_2, while it is totality with other models. The classification error of EB_2 may be caused by its instability when γ is close to ρ_1 or ρ_2. The classification error of other models highlights the lack of robustness to the baseline's variability of models with an analytic *a priori* on the baseline.

To conclude, this work proposed an estimated baseline model whose robustness to the baseline variability has been demonstrated in terms of parameters estimation error and healthy/tumoral classification.

ACKNOWLEDGMENTS

This work has been funded by LABEX PRIMES (ANR-11-LABX-0063) of Université de Lyon, within the program "Investissements d'Avenir" (ANR-11-IDEX-0007) operated by the French National Research Agency (ANR) and carried out within the framework of France Life Imaging (ANR-11-INBS-0006).

REFERENCES

[1] Li, Y. et al., "Intraoperative fluorescence-guided resection of high-grade gliomas: a comparison of the present techniques and evolution of future strategies.," *World Neurosurg.* **82**, 175–185 (Jul 2013).

[2] Liu, J. T. C. et al., "Trends in Fluorescence Image-Guided Surgery for Gliomas," *Neurosurgery* **75**, 61–71 (Jul 2014).

[3] Valdés, P. A., Roberts, D. W., Lu, F.-K., and Golby, A., "Optical technologies for intraoperative neurosurgical guidance," *Neurosurg. Focus* **40**, E8. (Mar 2016).

[4] Maugeri, R. et al., "With a Little Help from My Friends: The Role of Intraoperative Fluorescent Dyes in the Surgical Management of High-Grade Gliomas," *Brain Sci.* **8**, 31. (Feb 2018).

[5] Bander, E. D. et al., "Advances in glioblastoma operative techniques," *World neurosurgery* **116**, 529–538 (2018).

[6] Stummer, W. et al., "Technical principles for protoporphyrin-IX-fluorescence guided microsurgical resection of malignant glioma tissue," *Acta Neurochir.* **140**(10), 995–1000 (1998).

[7] Alston, L. et al., "Nonlinear relation between concentration and fluorescence emission of protoporphyrin IX in calibrated phantoms," *J. Biomed. Opt.* **23**, 097002 (Sep 2018).

[8] Black, D. et al., "Characterization of autofluorescence and quantitative protoporphyrin IX biomarkers for optical spectroscopy-guided glioma surgery - Scientific Reports," *Sci. Rep.* **11**, 1–12 (Oct 2021).

[9] Leclerc, P. et al., "5-ALA induced PpIX fluorescence guided surgery of gliomas: comparison of expert and machine learning based models," in [*Clinical and Translational Neurophotonics 2020*], Madsen, S. J., Yang, V. X. D., and Thakor, N. V., eds., **11225**, 30 – 33, International Society for Optics and Photonics, SPIE (2020).

[10] Leclerc, P. et al., "Machine learning-based prediction of glioma margin from 5-ALA induced PpIX fluorescence spectroscopy - Scientific Reports," *Sci. Rep.* **10**, 1–9 (Jan 2020).

[11] Montcel, B. et al., "Two-peaked 5-ALA-induced PpIX fluorescence emission spectrum distinguishes glioblastomas from low grade gliomas and infiltrative component of glioblastomas," *Biomed. Opt. Express* **4**, 548–558 (Apr 2013).

[12] Montcel, B. et al., "5-ALA-induced PpIX fluorescence in gliomas resection: spectral complexity of the emission spectrum in the infiltrative compound," in [*Neurophotonics*], **8804**, 880409, International Society for Optics and Photonics (Jun 2013).

[13] Abi Haidar, D. et al., "Spectral and lifetime domain measurements of rat brain tumors," *Biomed. Opt. Express* **6**, 1219–1233 (Apr 2015).

[14] Alston, L. et al., "5-ALA induced PpIX fluorescence guided surgery: a clinical study of spectral complexity in healthy tissues and margin boundaries in high and low grade gliomas," in [*Clinical and Preclinical Optical Diagnostics II*], Brown, J. Q. and van Leeuwen, T. G., eds., **11073**, 92 – 95, International Society for Optics and Photonics, SPIE (2019).

[15] Alston, L. et al., "Spectral complexity of 5-ALA induced PpIX fluorescence in guided surgery: a clinical study towards the discrimination of healthy tissue and margin boundaries in high and low grade gliomas," *Biomed. Opt. Express* **10**, 2478–2492 (May 2019).

[16] Haidar, D. A., Leh, B., Zanello, M., and Siebert, R., "Spectral and lifetime domain measurements of rat brain tumors," *Biomed. Opt. Express* **6**, 1219–1233 (Apr 2015).

[17] Jonin, C. et al., "Two photon excited fluorescence and hyper rayleigh scattering of protoporphyrin ix," *Journal of Photochemistry and Photobiology A: Chemistry* **402**, 112812 (2020).